ChemPubSoc Europe

DOI: 10.1002/slct.201601271

Chemistry SELECT Full Papers

Materials Science inc. Nanomaterials & Polymers

Non-Hydrothermal Synthesis of Cu(I)-Microleaves from Cu (II)-Nanorods

Tukhar Jyoti Konch,[a] Mukesh Sharma,[a] Lanka Satyanarayana,[b] Anil Hazarika,[c] Galla V. Karunakar,[d] and Kusum. K. Bania*[a]

Simultaneous transformation of structural morphology, material dimension and oxidation state of Cu (II)-nanorod was achieved with 3-(Triethoxysilyl)propylamine, (APTS) and 4-nitrobenzaldehyde (4-NB) under non-hydrothermal condition. Morphology of the modified Cu(I) material was found to resemble with the leaf of colocasea. Conversion of a Cu(II) based nono-material to a Cu(I)-based micro-material was confirmed from EPR, MAS- NMR and cyclic voltametric (CV) study. BET-surface area, Raman signal intensity and thermal stability of the Cu(I)-microleaf was greatly enhanced due to presence of Cu-O–Si linkage. Both the Cu(II) and Cu(I) material were found to be effective catalyst systems for nitro-aldol reaction as well as catalytic oxidation of methylene blue (MB) dye in presence of H_2O_2. High %yield (> 90%) of nitro-aldol product was obtained with both the catalyst. Catalytic reaction under microwave irradiation was found to bring substantial decrease in reaction time. Cu (II)-material was however not recyclable because of its soft nature. While the Cu(I)-microleaf was recycled upto four consecutive cycles. These materials were found to degrade methylene blue dye within 20 min in presence of H_2O_2 but in absence of light. Dark phase catalytic oxidation of MB was monitored both *via* UV-vis and cyclic voltametric study.

Introduction

Development of nano-based materials and nanotechnology has recently brought a new renaissance in designing of newer materials for various applications.[1] Starting from its applications in house utensils to the drug delivery, nanomaterials have captured a wide range of research area like energy conversion and storage, chemical manufacturing, biological applications, and environmental technology.[2–13] Catalysis by nanoparticles or nanomaterials is one of the important aspects where researchers from both industries and academics are paying much interest.[14,15] So far various transition metal like gold (Au),[16] platinum (Pt),[17] palladium (Pd),[18] silver (Ag)[19] etc have been well explored as nanocatalyst for transforming various organic reactions. In this context, Cu-containing nanomaterials or nanoparticles are gaining much interest in catalysis due to the high abundances of copper and low cost synthetic method. Cu-nanoparticles either in its oxide form CuO or as hydroxide, $Cu(OH)_2$ or as sulphides, CuS has recently been employed as catalyst in various type of catalytic reactions.[20]

Cu-nanomaterials or nanoparticles are mostly synthesized by hydrothermal or solvothermal methods using some suitable reducing and stabilizing agents.[20] In many cases Cu-salts with different counterions are taken as source of copper.[20] These methods however have some limitations i.e. control over the growth of nanoparticles. Temperature, pressure, molar ratios, nature of counterions and stabilizers plays vital role in architecting the surface morphology of Cu-nanomaterials.[21] So in recent years researchers are trying to synthesize Cu-based nanomaterials using some metal complex as precursors. Liu et al.[22] has synthesized CuS from Cu-thiourea complex, Yao et al.[23] has obtained CuS from Cu(I) complex of thioacetamide.

Researchers seemed to be more focused towards the hydrothermally synthesized Cu-nanomaterials in low oxidation state. But less emphasis has been given on synthesis of Cu(I) and Cu(II) material without following the conventional hydrothermal process. A very few reports are available for synthesis of Cu(II) complex in its nanodimension.[24,25] The objective of the present work is therefore to synthesize a Cu(II)- complex in nanoscale and its conversion to a Cu(I)-based material *via* a non-hydrothermal process. Such method will reduce the number of steps involved in hydrothermal process. It will also avoid the use of specific stabilizing agent and also the toxic reducing agents resulting in a development of one green method. Further, as one dimensional nanomaterials also finds high applications in optics, magnetism, and microsystems

[a] *T. J. Konch, M. Sharma, Dr. K. K. Bania*
Department of Chemical Sciences
Tezpur University
Assam, 784028, India
Tel: 09859929360
E-mail: kusum@tezu.ernet.in
bania.kusum8@gmail.com
[b] *Dr. L. Satyanarayana*
Center for NMR and Structural Chemistry
Indian Institute of Chemical Technology
Uppal Road, Tarnaka, Hyderabad, Telangana 500007, India
[c] *A. Hazarika*
Sophisticated Analytical Instrumentation Centre (SAIC)
Tezpur University
Assam, 784028, India
[d] *Dr. G. V. Karunakar*
Division of Crop Protection Chemicals
Indian Institute of Chemical Technology
Uppal Road, Tarnaka, Hyderabad, Telangana 500007, India

Supporting information for this article is available on the WWW under http://dx.doi.org/10.1002/slct.201601271

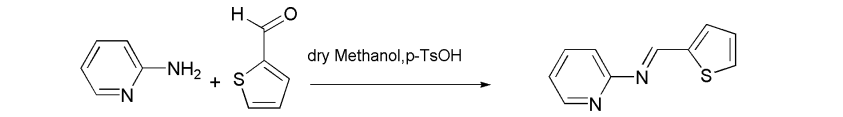

2-amino pyridine thiophene 2-carbaldehyde (*E*)-*N*-((thiophen-2-yl)methylene)pyridin-2-amine

Scheme 1. Synthesis of ligand precursor.

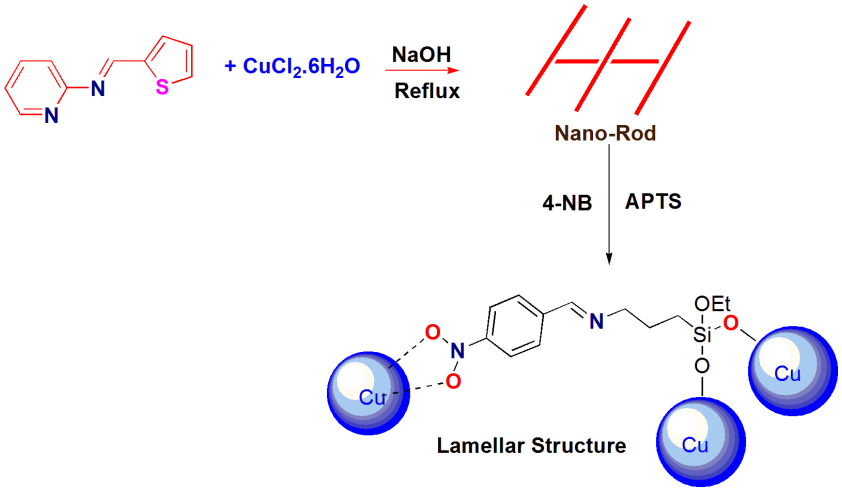

Scheme 2. Preparation of Cu(II) Nano-rod and Cu(I)-Microleaf.

electronics so such nano-complexes could contribute in the expansion of those fields.[26,27]

Cu-Schiff base complex are important class of metal complex which has gained lot of application in the field of catalysis.[28] From our group we have reported for supported Cu-Schiff base complexes encapsulated in zeolite-Y.[29] Those catalysts were also used as recyclable chiral catalyst for asymmetric Henry reaction.[28,29] However, to best of our knowledge Cu(I)/Cu(II)-Schiff base metal complexes in nano or micro dimensions are not explored for such reaction.[30] So herein we synthesized rod shape Cu-Schiff base complex in nano form and they were further modified with silicon. Both catalysts were then used for promoting nitro-aldol reaction and catalytic oxidation of methylene blue.

Experimental Section

Synthesis of Schiff Base Ligand

Schiff base ligand as shown in Scheme 1 was prepared following the reported procedure.[31] Equimolar quantities of 2-thiophenecarboxaldehyde, (10 mmol) and 2-aminopyridine (10 mmol) were refluxed in dry methanol with catalytic amount of *p*-toluenesulfonic acid monohydrate for 24 h. The desired product was obtained in 75% yield after separation with column chromatography. Product was characterized by ^{1}H NMR and ^{13}C NMR. ^{1}H NMR (Methanol-D_3, 400 MHz) δ 9.11 (s, 1H), 8.39 (d, 1H), 7.84 (td, 1.8 Hz, 1H), 7.41 (m, 2H), 7.28 (m, 3H) ppm. ^{13}C NMR (Methanol-D_3, 100 MHz) δ 160.9, 156.5, 146.3, 138.8, 134.9, 131.9, 128.0, 125.1, 121.8, 118.6 ppm.

Preparation of Cu(II)-Shiff Base Nanorods, Cu(II)-SB-NR

In a 20 ml round bottom (RB) flask, 2 mmol of the synthesized ligand was dissloved in methanol. To this solution, 3 mmol of copper (II) choloride dihydrate ($CuCl_2$. $2H_2O$) dissolved in acetronitrile was added in dropwise manner, untill the solution become green in colour. After refluxing the green solution for 4 hours in alkaline condition (in presence of NaOH) resulted in a sky blue ppt, Scheme 2. The sky blue ppt was filtered and dried for further characterization. Herein we designated this material as Cu(II)-SB-NR.

Preparation of Cu(I) Microleaf, Cu(I)-SB-NR@Si

In a RB flask, 4-nitrobenzaldeyde (4-NB) and 3-(Triethoxysilyl)propylamine, (APTS) were taken in 1:1 ratio and stirred for 3 hours in inert atmosphere. Cu(II)-SB-NR) was then added to the system with a spatula without distrubing all other reaction condtions, Scheme 2. After a duration of 10 hours a sticky brownish ppt appears which was extracted with dry toluene. A very light brownish and slightly crystalline solid compound was obtained. The solid material was then subjected to Soxhlet extraction to remove any unreacted substances. The purified compound was dried in vaccum for further use. Compound is designated as Cu(I)-SB-NR@Si.

General Procedure for Asymmetric Henry Reaction

4-nitrobenzaldehyde (4-NB) (5 mmol) was taken in a typical round bottom flask used for microwave treatment and 10 mg of the catalyst was added. The resulting mixture was stirred for few minutes and nitromethane (5 mmol) was added dropwise into it. The whole reaction mixture was then subjeted to mirowave irradiation with 50% power (425W) at 31 °C for 15 min in a scientific multimode microwave reactor equipped with digital power and temperature control unit. After irradiation with microwave the reaction mixture was magnetically stirred for 2 hrs at room temperature. Formation of product was confirmed by observing the progress of the reaction using TLC. Resultant nito-aldol produt was seperated by washing the reaction mixture for several times with 9:2 mixture of hexane ethyl acetate solution.

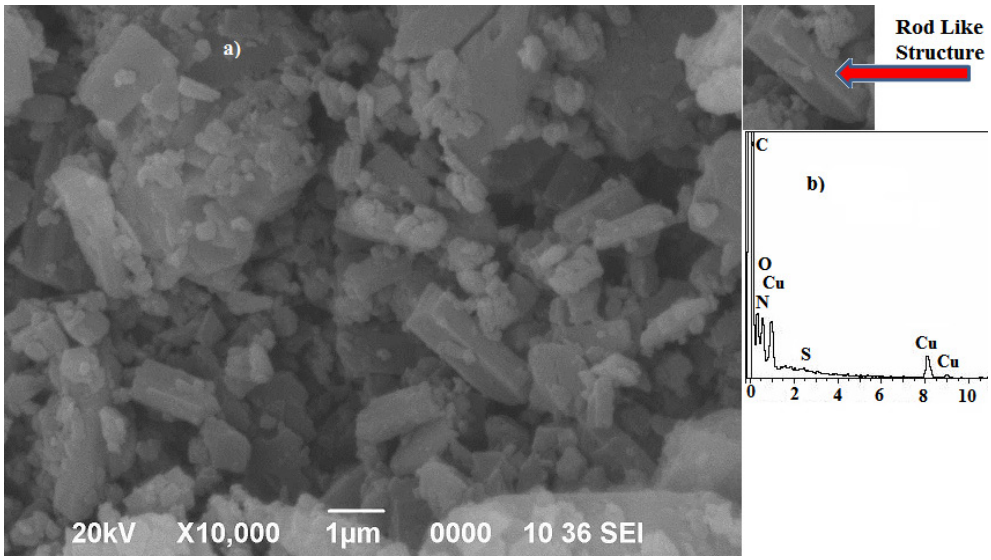

Figure 1. a) SEM-image of Cu(II)-SB-NR b) EDX analysis.

Results and Discussion

The morphology of the synthesized materials were examined by SEM and TEM study. SEM image of Cu(II)-SB-NR shows rod like structure in the nanometer range, Figure 1a. Presence of Cu, S, N and O were confirmed from EDX analysis, Figure 1b. TEM image shown in Figure 2 shows beautiful rod like structure

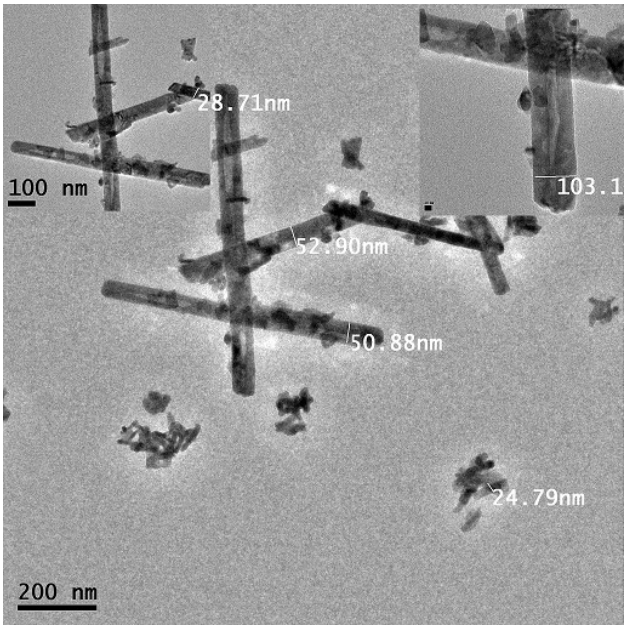

Figure 2. TEM image of Cu(II)-SB-NR showing rod-like structure.

for Cu(II)-SB-NR of variable dimension. SEM image of Cu(I)-SB-NR@Si shows lamellar structure in the micrometer range, Figure 3a. The morphlology of Cu(I)-SB-NR@Si rsembles with leaf of colocasia Figure 3b and hence we called it microleaf. Transformation of the rod like nanostructure of Cu-Schiff base complex to a microleaf like structure on modification with 4-nitrobenzaldeyde and 3-(Triethoxysilyl)propylamine (APTS) is attributed to linkage of the silicon moiety.

PXRD pattern of Cu(II)-SB-NR shows five highly intense peak at 2θ value of 8.3°, 9.9°, 12°, 13.3° and 16.5° characteristics of Cu-Schiff base complex in nanoform, Figure 4a and Figure 4b. However, as similar PXRD pattern were not available in the literature, so it was difficult for us to exactly compare the PXRD pattern.[31] But it matches well with recently reported PXRD pattern of Cu(II) Schiff base complex in nanodimension.[30,33] So it can be concluded that probably the nanostructured Cu(II)-SB-NR material is formed *via* extension of linkage in the co-ordination sphere of Cu-Schiff base complex leading to nano-rod like structure. PXRD pattern of Cu(I)-SB-NR@Si also resembles well with those observed for mesoporous silicon based compounds, Figure 4c. The broad signal at $2\theta = 21^\circ$ due to amorphous silica further confirmed the modification of Cu-nanorods with silicon based compounds.[32] The other weak peaks below 2θ value of 20° and in between $2\theta = 30\text{-}40^\circ$ corresponds to Cu(II)-SB-NR. Surface area of the Cu(II)-SB-NR was found to be very less 7 m^2/g while it was 43 m^2/g for Cu(I)-SB-NR@Si. BET isotherm of the Cu(I)-SB-NR@Si represent a Type IV isotherm typical of mesoporous siliceous material, Figure S1a. BJH pore size distribution gives a wide pore size distribution within a range of 6–60 nm charactersitics of mesoporous materaial of hierachical structure, Figure S1b. Increase in surface area and presence of characteristic Type IV isotherm clearly indicates for successful transformation of Cu-Schiff base nanorod material to a porous material. From TGA analysis it was found that Cu(II)-SB-NR nanorod has degradations in the range of 170–280 °C due to dehydration of surface based water molecules and decomposition of ligand moiety, resulting in a weight loss up to 55%, Figure S2a. But in Cu(I)-SB-NR@Si initial weight loss for the same degradation starts at a slightly higher temperature i.e. from 186 °C and terminates at about 360 °C, with a concomitant weight loss up to only 25%,

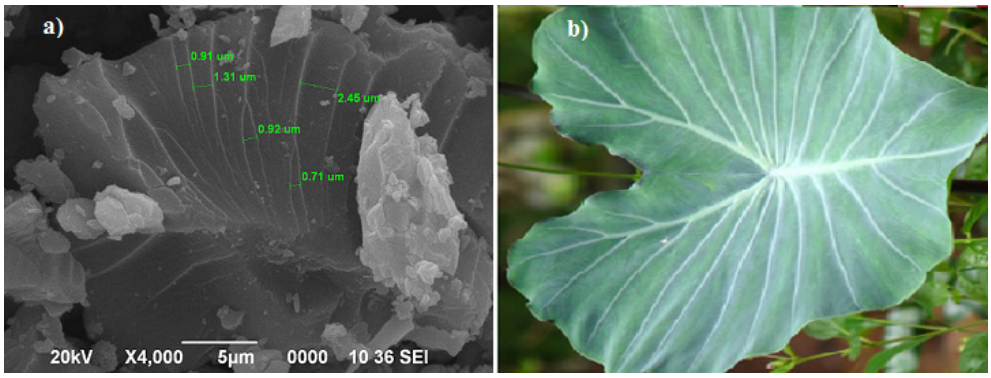

Figure 3. a) SEM image of Cu(I)-SB-NR@Si and its comparison with b) leaf of colocasia.

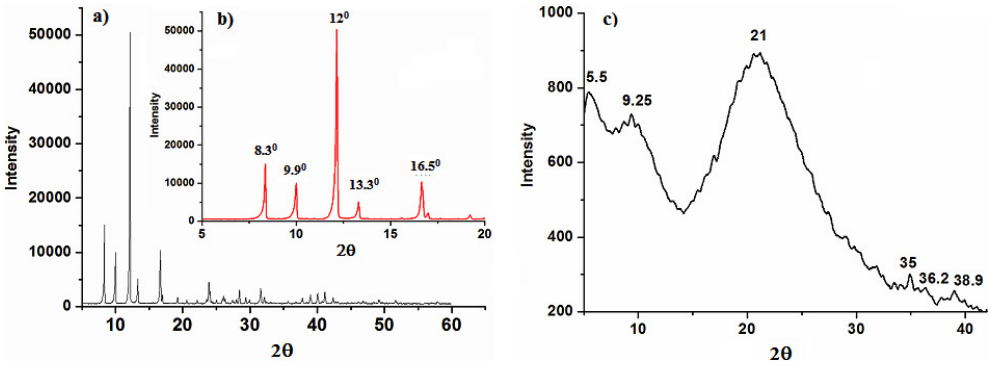

Figure 4. a) PXRD pattern of Cu(II)-SB-NR b) inset shows the five charactristic intense peak c) PXRD pattern of Cu(I)-SB-NR@Si.

Figure S2b. The second peak in the temperature range of 380–440 °C might occurs due to the delinking of Cu-Silicon, Figure S2b. The silicon based materials acts as a support to the Cu(II)-SB-NR and thereby enhances the thermal stability.

FT-IR spectrum of the Cu(II)-SB-NR is shown in Figure 5a. Presence of characteristic C=N (1639 cm^{-1}), C–H (1434 cm^{-1}), C=C (1320 cm^{-1}) and C=S (1177, 676, 623) bands confirmed the formation of Cu(II)-Schiff base complex.[34] A doublet at 3323 and 3475 cm^{-1} suggest for bridging –OH group.[35] Co-ordination of S and N-atom to metal centre was confirmed from the FIR analysis with the presence of characteristic band at 350 and 622 cm^{-1}, Figure 5b. Band in between 437–521 in the FIR spectrum was attributed to Cu–O bond related to hydroxy bridged copper compounds, Figure 5b.[34] Cupric oxide also shows absorption in this region. Band at 263 cm^{-1} was due to Cu–N asymmetric vibrations while that at 172 cm^{-1} could be due to N–M-N vibration,[35] Figure 5b. In case of Cu(I)-SB-NR@Si, apart from C=N, C=S and C–H vibrational band, strong signals at 1113 and 1017 cm^{-1} confirmed for Si–O linkage through triethoxy silanes, Figure 5c. Band at 1592 cm^{-1} was due to –C=N bond formed *via* condensation of the $–NH_2$ group of 3-(triethoxysilyl) propylamine with aldehydic group of 4-nitrobenzaldehyde (4-NB). Two sharp signals at 1511 and 1342 cm^{-1} were due to the N–O stretching vibration of NO_2 group of 4-NB.[34] Similar vibrational bands were observed in the Raman spectra characteristic of the Cu-Schiff base complex, Figure 5d and 5e. Bands at 886–887 cm^{-1} were due to CH_2-vibration which appeared very sharp and as doublet in case of Cu(I)-SB-NR@Si, Figure 5e. Peaks between 1000–1200 cm^{-1} in Cu(I)-SB-NR@Si were attributed to Si–O linkage, Figure 5e.[29] Comparison of Raman intensity of nanorod structure with that of the Si-modified Cu-Schiff base having lamellar morphology; it was observed that Raman signals were greatly enhanced due to surface enhancement. Increase in Raman signal intensity and presence of Si–O bond vibration strongly suggest for surface modification of Cu(II)-Schiff base nanorods.

Room temperature EPR spectra of Cu(II)-SB-NR shows broad signals in both low and high magnetic field with a sharp line at 500 mT characteristic of dimeric or polymeric Cu(II)-complexes, Figure 6a.[36] Absence of any signal nearly at 330–340 mT indicates for the non-existence of any monomeric impurity.[37] The values obtained for spin Hamiltonian parameters are g_{II} = 2.072; $g_{\perp}$ = 2.314; g_{av} = 2.193 matches well with similar dimeric Cu(II)-complex.[38] Cu(I)-SB-NR@Si did not exhibited any EPR signal confirming the change in oxidation state from Cu(II) to Cu(I) state. Cyclic voltammogram of the nanorod structure shows a cathodic peak at –0.207 V due to Cu(II)/Cu(I) process and sharp anodic signals at 0.49 V, due to Cu(I)/Cu(II) process, Figure 6b. These potential values resembles well with those of Cu(II) complex with N_2S_2 ligand.[39] Cu(I)-SB-NR@Si material shows a quasi reversible cyclic voltammogram with the anodic signal at –0.61 V and cathodic signal at –0.96 V, Figure 6c. These peaks correspond to successive Cu(II) reduction processes.[40] The difference in the redox potential value clearly signifies the change in the oxidation state from Cu(II)→Cu(I) in Cu(I)-SB-NR@Si.

^{13}C and ^{29}Si solid state NMR analysis further confirmed the diamagnetic nature of Cu(I)-SB-NR@Si. In the ^{13}C NMR spectra (Figure 7a) signals were observed at 168, 158 and 151 ppm characteristic of three different carbon atom labelled as **1**, **2**

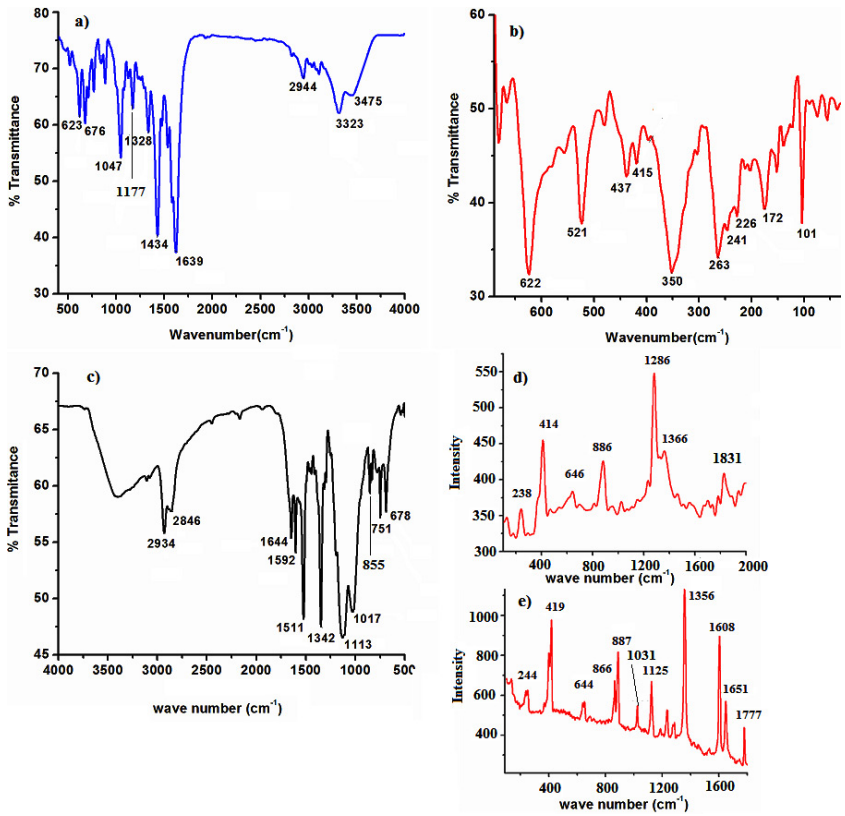

Figure 5. FTIR spectra of a) Cu(II)-SB-NR b) FIR-spectra of Cu(II)-SB-NR c) FTIR spectra of Cu-SR-NR@Si d) Raman spectra of Cu(II)-SB-NR and e) Raman spectra of Cu(I)-SB-NR@Si.

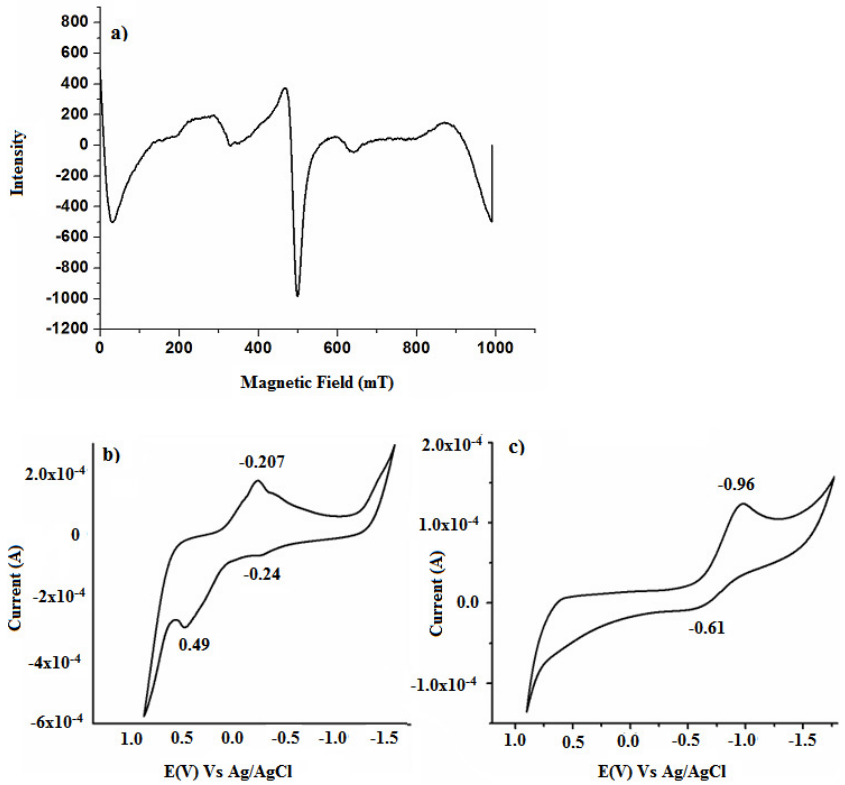

Figure 6. a) Room temperature EPR-spectra of Cu(II)-SB-NR. Cyclic voltammogram of b) Cu(II)-SB-NR and c) Cu(I)-SB-NR@Si..

and **3** in Figure 8. Peaks at 133-ppm were due to aromatic carbon atoms. Absence of any signal above 180 ppm confirmed the absence of free aldehydic group. Other significant peaks were observed at 74 and 21 ppm corresponding to carbon

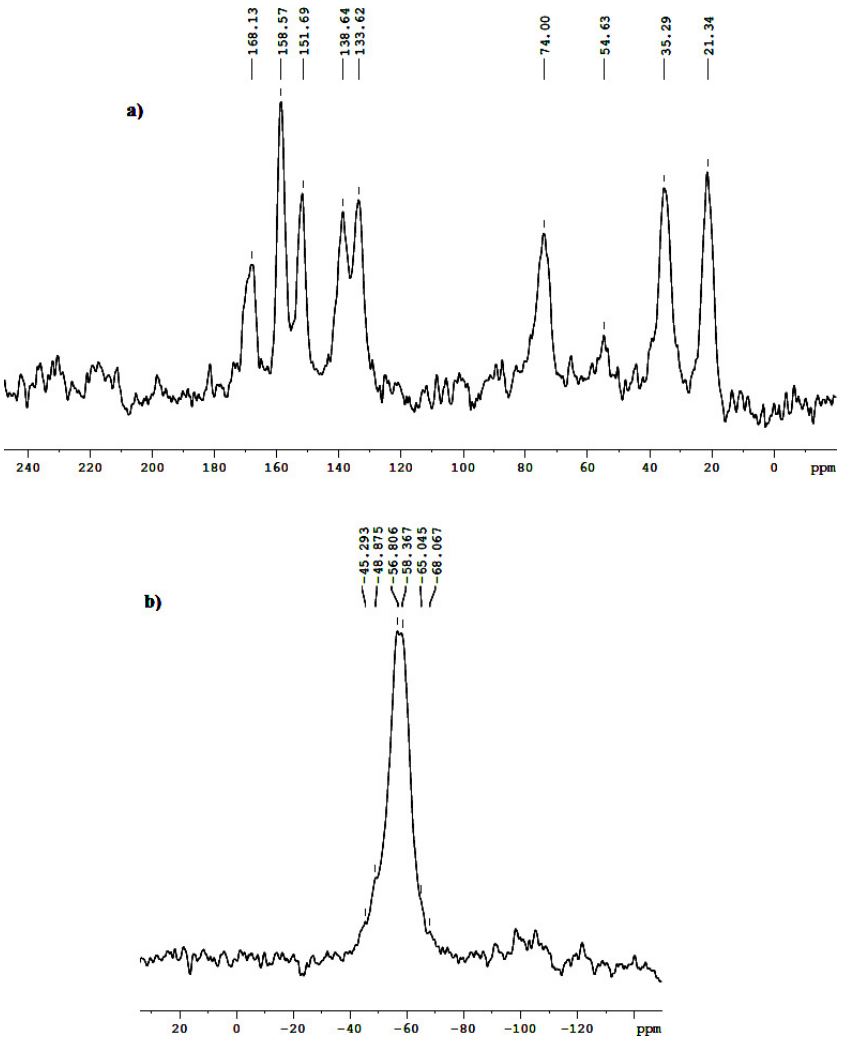

Figure 7. Solid state a)^{13}C and b) ^{29}Si NMR of Cu(I)-SB-NR@Si.

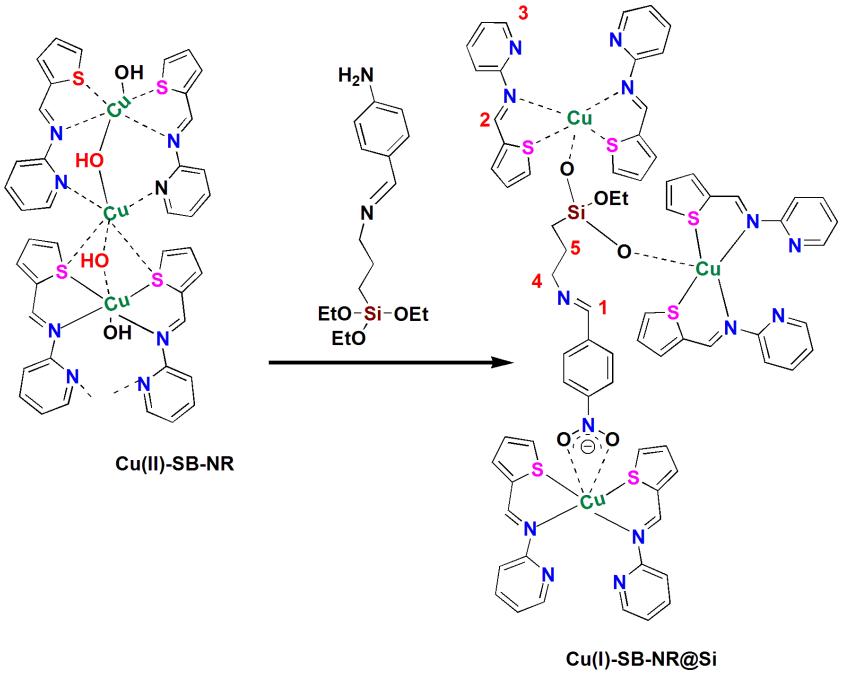

Figure 8. Expected structural arrangement in Cu(II)-SB-NR and Cu(I)-SB-NR@Si.

Table 1. Results of Henry reaction with 4-nitro-benzaldehyde and nitromethane using 10 mg of Cu(II)-SB-NR catalyst in different solvent conditions and under different reaction condition

	At Room Temperature in Normal Magnetic Stirring		MW (15 min) + Magnetic Stirring	
Solvent	Time	% Yield	Time	Yield
Ethanol	12	65	2	72
Methanol	12	57	2	62
DCM	12	59	2	61
Acetonitrile	12	80	2	90
DMF	12	12	2	20
THF	12	10	2	15
Toluene	12		2	
CCl_4	12	trace	2	

atom labelled as **4** and **5**, Figure 8.[41] Signal at 54 was due to α carbon atom of ethoxy group of APTS.[41] Peak at 35 ppm might come from trace amount of unreacted APTS present on the surface. ^{29}Si NMR of the sample was found to be dominated by the signal at −56 and-58 ppm identified with two Si–O attachments to the nanorod surface, Figure 7b. A much smaller peak seen at −49 ppm and −65 and −68 ppm, attributed to one and three Si–O linkage respectively to the surface.[41] Another much smaller peak at −45 ppm was due to the ^{29}Si chemical shift of neat, liquid APTS remained as trace amount. Since the intensity of ^{29}Si-NMR signal is conquered by the signal at −56 and −58 ppm so it can be concluded that out of the three -OEt group in APTS two are involved in forming Si–O linkage with Cu(II)-SB-NR while the other –OEt group remain unhydrolyzed.

Based on the above analysis and various mechanism suggested by other researchers,[42–44] we proposed the likely structure of Cu(II)-SB-NR and Cu(I)-SB-NR@Si as shown in Figure 8. On treating with APTS, the Cu(II) nanorod first get converted to Cu(I)-SB-NR@Si polymeric nanooparticles[45,46] which spontaneously gets aggregates to form Cu(I)-SB-NR@Si micro particles with lamellar structure. The aggregation of nanoparticles to supra or micro particles is a general phenomenon in nanomaterials.[47,48]

In the DRS spectra of Cu(II)-SB-NR showed a broad shoulder around 350 nm and reached a minimum around 500 nm, but not zero intensity, Figure S3a. The absorbance never reaches zero intensity but rises for longer wavelengths again, is thought to come from the free-carrier intra-band absorbance.[22] In other words we can say electron in the valence band is raised into higher energy conduction band within the same band due to quantum confinement which in turn is responsible for the free carrier intra-band transition. This is of course possible when the material will have particles or atoms in nanodimensions. Such characteristic DRS spectra were previously observed in CuS nanomaterials having nanorod structure.[22] In case of Cu(I)-SB-NR@Si since material has transformed from a nanodimension to micro-meter range quantum confinement almost gets diminished, so there is no free carrier intra-band transition and hence absorbance intensity approaches zero with increasing wavelength up to 658 nm, Figure S3b.

The Cu-Schiff base nanorod also exhibited a strong emission peak at 396 nm and two broad weak peaks at around 432 and 462 nm when excited at 280 nm, Figure S4. This suggests that Cu(II)-SB-NR has strong UV emission peak at 400 nm and weak blue emission peak at 432 and 462 nm. PL-spectra resemble well with those of CuS nanostructured materials.[22] Since our synthesized Schiff base ligand contains both S and N as co-ordinating site therefore, it can be concluded Cu is strongly bonded to S compared to N-atom.

Catalytic Study

Nitro-Aldol Reaction

In recent times Cu-Schiff base metal complexes has been well explored as catalyst for nitro-aldol reaction.[28,29] Cu-Schiff base complexes either in homogeneous or in heterogeneous phase acts as excellent catalyst for such organic transformation. However, no report is available in literature where Cu-Schiff base nano-catalyst is being used for catalytic formation of nitro-aldol product. Since nanomaterials are found to have good catalytic activity, so herein we tried to develop a new reusable catalyst for nitro-aldol reaction.

Taking 4-NB and nitromehane (CH_3NO_2) as reactant the nitro-aldol reaction was performed with 10 mg of Cu(II)-SB-NR at room temperature in ethanol as solvent. From our previous experience we observed that nitro-aldol reaction proceeds well at low temperature.[28,29] With the nanocatalyst, Cu(II)-SB-NR nitro-aldol product was achieved in good yield (65%) after 12 h at room temperature. Hence reaction was tested in different solvent system at room temperature (25 °C). Results of the catalytic reaction in different solvent are depicted in Table 1. In non-polar solvents reaction was found to be sluggish leading to low or no product formation. Acetonitrile (CH_3CN) was found to be the best solvent under the prevailing conditions giving 80% yield, Table 1.

In recent times catalytic reaction under microwave irradiation has found to be much beneficial in terms of green perspective and reaction time.[49,50] So we also carried out the reaction under microwave irradiation. After irradiating the reaction mixture initially with microwave for 15 min followed by normal room temperature magnetic stirring for 1 h 45 min nitro-aldol product was achieved in good yield (90% in acetonitrile), Table 1. As the reaction time was reduced from 12 h to 2 h because of the initial irradiation with microwave so we performed the Henry reaction taking different substrate under microwave condition and the results are given in Table 2.

As Cu(II)-SB-NR nanocatalyst was found to show good catalytic activity towards the Henry reaction under microwave

Table 2. Results of the Henry reaction with various aldehydes and nitromethane using 10 mg in presence of Cu(II)-SB-NR and Cu(I)-SB-NR@Si catalyst under microwave condition.

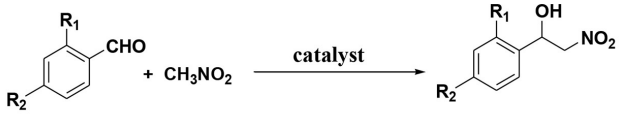

1a R_1= H, R_2 = H
1b R_1= H, R_2 = NO_2
1c, R_1= NO_2, R_2= H
1d, R_1= H, R_2= CH_3
1e, R_1=H R_2= OH
1f, Napthaldehyde

2a R_1= H, R_2 = H
2b R1= H, R_2 = NO_2
2c, R_1= NO_2, R_2= H
2d, R_1= H, R_2= CH_3
2e, R_1=H R_2= OH
2f, 1-(naphthalen-6-yl)-2-nitroethanol

Reactant	Product	Cu(II)-SB-NR Time(h)	%Yield	Cu(I)-SB-NR@Si Time (min)	%Yield
1a	2a	2	84	45	86
1b	2b	2	90	45	94
1c	2c	2	80	45	92
1d	2d	2	78	45	81
1e	2e	2	72	45	78
1f	2f	2	82	45	84

Reactions are conducted at 5 mmol scale employing 5 equiv of nitromethane in acetonitrile and 10 mg of catalyst. All the reactions were carried out after irradiating with microwave for 15 min.

Catalytic Degradation of Methylene Blue

As the synthesized materials were found to have good photoluminescence so we also studied the catalytic behaviour of the material towards MB degradation in the presence of H_2O_2 as oxidant. For the catalytic study studies, we took 40 mL of 2×10^{-5} (M) MB aqueous solution in a beaker and there we add 10 mg of Cu (II)-SB-NR. The resulting solution was stirred in dark and the UV-vis absorption spectrum was recorded after an interval of 5 min. UV-vis spectrum shows characteristic decrease

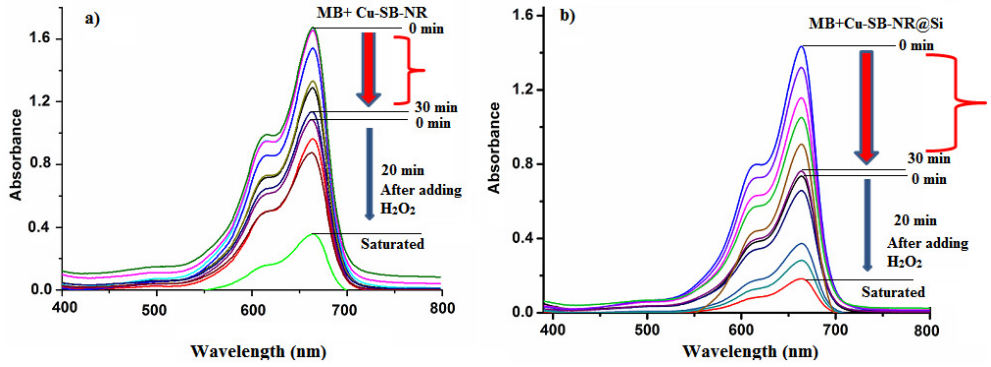

Figure 9. Change in absorption band at ~664 of MB after addition of catalyst and H_2O_2 a) with Cu(II)-SB-NR catalyst b) with Cu(II)-SB-NR@ Si catalyst.

irradiation followed by room temperature magnetic stirring so we further studied the catalytic activity Cu(I)-SB-NR@Si. It was observed that Cu(I)-SB-NR@Si in microleaf form gives much better catalytic activity. Further, the reaction time gets reduced to 45 min (15 min microwave + 30 min stirring), Table 2. Difference in catalytic activity can be attributed to morphological distinction of the complexes. Moreover, as the surface area of Cu(I)-SB-NR@Si was almost six times greater than Cu(II)-SB-NR, so that might lead to substantial difference in the catalytic performance. Results of the nitro-aldol reaction performed with Cu(I)-SB-NR@Si are given in Table 2

Besides the high catalytic activity, Cu(I)-SB-NR@Si has certain other advantages over Cu(II)-SB-NR. Cu(II)-SB-NR was difficult to regenerate after reaction as it gets sparingly soluble in solution after microwave irradiation due to its soft nature. So we could not recycle the catalyst. However, Cu(I)-SB-NR@Si was quite stable and gets easily precipitates out after completion of the reaction. The catalyst was recycled without any loss in catalytic activity for four consecutive cycles.

in absorption band at ~664 nm due to the adsorption of MB on the nano-catalyst. However, this decrease was only observed upto 6th reading and 30 min of stirring the reaction mixture, Figure 9a. This happened probably the catalyst reached the saturation limit and achieved equilibrium between the adsorbate and sorbent i.e. adsorption equilibrium was created in between MB and Cu-catalyst after 30 min. The absorbance value was found to decrease from 1.63 to 1.13 a difference of 0.50 i.e. the catalyst adsorbed nearly ~50% of MB. Then, we added 1 mL of H_2O_2 to the reaction mixture and the solution was stirred in dark, Figure 9a. On monitoring the UV-vis spectrum after addition of peroxide there occurred a sharp decrease in absorption spectrum and absorbance value decreases upto 0.33 within 20 min, Figure 9a. After this no further decrease in absorbance value was observed. The decrease in absorbance value of MB after addition of peroxide can be attributed to degradation of adsorbed MB on the surface of nano-catalyst in presence of peroxide. While monitoring the same reaction process on the modified catalyst, Cu(I)-SB-NR@Si the saturation limit of adsorption of MB was found to be much more enhanced in comparison to Cu(II)-SB-

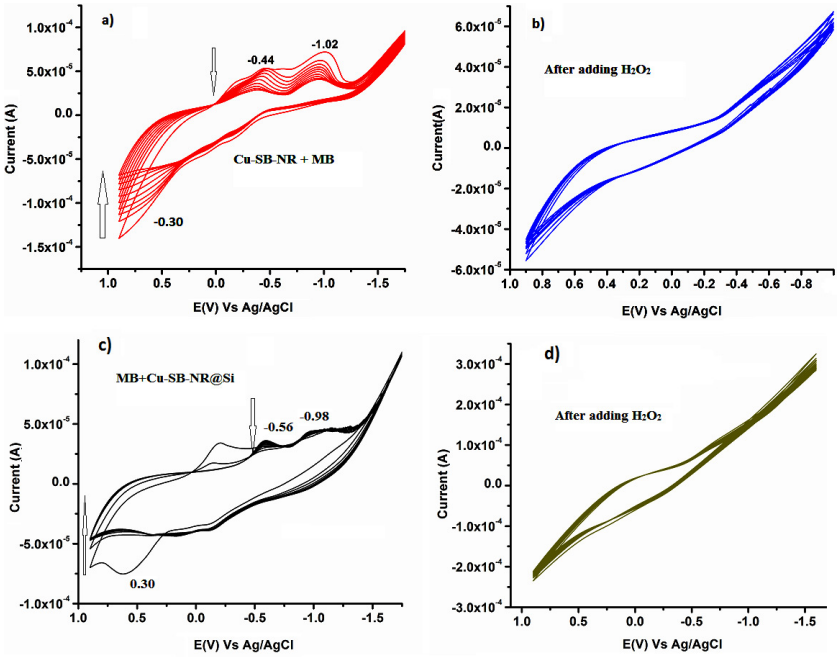

Figure 10. Cyclic voltammogram of a) MB + Cu(II)-SB-NR, b) MB + Cu(II)-SB-NR + H_2O_2, c) MB + Cu(I)-SB-NR@Si, d) MB + Cu(I)-SB-NR@Si + H_2O_2.

NR. Within the same interval of time the absorbance value was found to decrease from 1.43 to 0.75 a difference of 0.68 i.e. ~68% of MB was adsorbed on the catalyst surface, Figure 9b. High adsorption ability of Cu(I)-SB-NR@Si over Cu(II)-SB-NR could be attributed to high surface area associated with Cu(I)-SB-NR@Si catalyst. Further it was also observed that saturation limit of MB dye degradation in case of Cu(I)-SB-NR@Si was extended in comparison to Cu(II)-SB-NR catalyst, Figure 9b. This clearly indicates that the catalyst with high surface area can adsorb more and hence degradation process becomes more effective. MB-dye degradation test with both the catalysts was also monitored in presence of light. Initially degradation i.e. up to 20 min in presence of light was slightly higher (~2.5%) in comparison to those in dark. But after 20 min both the degradation rate in both dark and light phase becomes same. This gives a clear indication that in presence of either Cu(II)-SB-NR or Cu(I)-SB-NR@Si and H_2O_2 light is not required for degradation of MB. In other sense it can be said that Cu(II)-SB-NR or Cu(I)-SB-NR@Si simply acts as a catalyst rather than a photocatalyst.[21]

It is pertinent to mention herein that in presence of both the catalyst, the rate of adsorption of MB before the addition of H_2O_2 i.e. upto 30 min was not constant, Figure 9a and Figure 9b. This happened because of the non-uniformity in the surface of both the catalyst, Cu(II)-SB-NR and Cu(I)-SB-NR@Si. The MB degradation experiment was carried out under constant stirring, so surface exposure to the dye changes time by time. Cases arise where the less active sides of the catalyst are exposed to the dye in order to get adsorbed, resulting in relatively little decrease in MB concentration in after certain interval like at the first and forth reading Figure 9a and in third reading in Figure 9b. Similar results were also reported previously because of the change in the surface morphology of the catalyst.[51,52]

We also studied the interaction of MB with the Cu(II)-SB-NR and Cu(I)-SB-NR@Si *via* cyclic voltammetric study. MB in water with KCl as electrolyte shows two cathodic signals at −0.44 V and −1.19 V against Ag/AgCl as reference electrode and GCE (glassy carbon electrode) as working electrode. In presence of catalyst but in absence of light when the CV was run for 20 cycles we observed beautiful change in anodic and cathodic peak current, Figure 10a. Cathodic peak current was found to decrease gradually while the anodic peak current grows significantly. This clearly signifies the interaction of MB with the catalyst surface. After addition of peroxide no any anodic or cathodic peak were observed even after running for 20 cycles suggesting conversion of MB to some other redox inactive species, Figure 10b. In presence of Cu(I)-SB-NR@Si, besides the change in the peak current there also occurred shifting of peak potential values and a new cathodic peak appeared at −0.23 V which get disappeared after few cycles, Figure 10c. Shifting of peak potential values and appearance of new cathodic peak in the cyclic voltammogram clearly indicates the adsorption of MB on the soild catalyst. Both the anodic and cathodic peaks get disappeared after addition of peroxide leading to substantial degradation of MB, Figure 10d. Increase in anodic peak current confirms the oxidative behaviour of the catalysts towards the MB degradation process. In all the processes the basic cyclic voltammogram shape is the same, but with the modified microleaf structured catalyst better reduction in the cathodic peak current was observed with addition of hydrogen peroxide. It confirms the efficient oxidative behaviour of the modified catalyst in comparison to the other towards degradation of MB.

Conclusion

In summary we have been successful in designing a new Cu(II) containing nanomaterial having rod-like morphology. However,

thermal stability of the material was less. On modification with silicon based compounds the thermal stability, surface area and catalytic activity of the soft nanomaterial was greatly enhanced. Both nanorod Cu(II) Schiff base complex and modified materials acts as excellent catalyst in nitro-aldol reaction. Catalytic activities of the materials were more or less comparable with other reported Cu-nanocatlyst. Hence, without going for hydrothermal synthesis one can synthesize Cu-nanomaterials of suitable morphological structure

Supporting Information

Details of Physical measurements, BET isotherm and BJH pore size distribution, TGA analysis, DRS and PL-spectra of Cu(II)-SB-NR

Acknowledgements

KKB and MS thanks Science and Engineering Research Board, (SERB), Department of Science and Technology (DST), India for the financial grant (NO SB/EMEQ-463/2014). The authors thank Dr. Pabitra Nath, Department of Physics, Tezpur University and his research group for providing the Raman analysis. Authors also thank Prof. J. B. Baruah, Department of Chemistry, IIT Guwahati for providing the EPR analysis.

Keywords: Cu-Nanorod · Microleaf · Non-Hydrothermal Synthesis · Henry Reaction · Dye degradation

[1] M. C Roco, W. S. Bainbridge, *J. Nanopart. Res.* **2005**, *7*, 1–13.
[2] S. H. Cheng, M. C. Chen, C. H. Lee, J. S. Souris, F. G. Tseng, C. Y. Mou, C. S. Yang, C. T. Chen, L. Lo, *J. Mater. Chem.* **2010**, *20*, 6149–6157.
[3] B. Menaa, F. Menaa, C. Aiolfi-Guimaraes, O. Sharts, *Int. J. Nanotechnol.* **2010**, *7*, 1–45.
[4] V. Labhasetwar, *Curr. Opin. Biotechnol.* **2005**, *16*, 674–680.
[5] D. A. LaVan, T. McGuire, R. Langer, *Nat. Biotechnol.* **2003**, *21*, 1184–1191.
[6] K. Park, *J. Control Release* **2007**, *120*, 1–3.
[7] M. Siegrist, M. Cousin, M. Kastenholz, A. Wiek, *Appetite* **2007**, *49*, 459–466.
[8] S. Laurent, D. Forge, M. Port, A. Roch, C. Robic, L. Vander Elst, R. N. Muller, *Chem. Rev.* **2008**, *108*, 2064 – 2110.
[9] M. B. Gawande, P. S. Branco, K. Parghi, J. J. Shrikhande, R. K. Pandey, C. A. A. Ghumman, N. Bundaleski, O. Teodoro, R. V. Jayaram, *Catal.Sci.-Technol.* **2011**, *1*, 1653 – 1664.
[10] A. T. Bell, *Science* **2003**, *299*, 1688 – 1691.
[11] D. Wang & D. Astruc, *Chem. Rev.* **2014**, *114*, 6949 – 6985.
[12] H. C. Zeng, *Acc. Chem. Res.* **2013**, *46*, 226 – 235.
[13] V. Georgakilas, M. Otyepka, A. B. Bourlinos, V. Chandra, N. Kim, K. C. Kemp, P. Hobza, R. Zboril, K. S. Kim, *Chem. Rev.* **2012**, *112*, 6156 – 6214.
[14] S. D. Senanayake, D. Stacchiola, J. A. Rodriguez, *Acc. Chem. Res.* **2013**, *46*, 1702 – 1711.
[15] S. Bordiga, E. Groppo, G. Agostini, J. A. van Bokhoven, C. Lamberti, *Chem. Rev.* **2013**, *113*, 1736 – 1850.
[16] A. Corma, H. Garcia, *Chem. Soc. Rev.* **2008**, *37*, 2096–2126.
[17] S. Mostafa, F. Behafarid, J. R. Croy, L. K. Ono, L. Li, J. C. Yang, A. I. Frenkel, B. R. Cuenya, *J. Am. Chem. Soc.* **2010**, *132*, 15714–15719.
[18] Y. Li, X. M. Hong, D. M. Collard, M. A. El-Sayed, *Org. Lett.* **2000**, *2*, 2385–2388.
[19] X. Hu, J. Bai, H. Hong, C. Li, *Micropor. Mesopor. Mat.* **2016**, *228*, 224–230.
[20] M. B. Gawande, A. Goswami, F. X. Felpin, T. Asefa, X. Huang, R. Silva, X. Zou, R. Zboril, R. S. Verma, *Chem. Rev.* **2016**, *116*, 3722 – 3811.
[21] J. Kundu, D. Pradhan, *ACS Appl. Mater. Interfaces* **2014**, *6*, 1823 – 1834.
[22] J. Liu, D. Xue, *J. Mater. Chem.* **2011**, *21*, 223 – 228.
[23] Z. Yao, X. Zhu, C. Wu, X. Zhang, Y. Xie, *Cryst. Growth & Des.* **2007**, *7*, 1256–1261.
[24] W. Li, L. Lang, J. Dianzeng, C. Yali, X. Xinquan, *Chin. Sci. Bull.* **2005**, *50* 758–760.
[25] O. B. Ibrahim, M. A. Mohamed, M. S. Refat, *Can Chem Trans.* **2014**, *2*, 108–121.
[26] S. Saito, *Science* **1997**, *278*, 77–78.
[27] P. L. Mceuem, *Nature* **1998**, *393*, 15–18.
[28] K. K. Bania, G. V. Karunakar, B. Sarma, R. C. Deka, *ChemPlusChem* **2014**, *79*, 427–438.
[29] K. K. Bania, G. V. Karunakar, K. Goutham, R. C. Deka, *Inorg. Chem.* **2013**, *52*, 8017–8029.
[30] W. Wang, Q. Chen, Q. Li, Y. Sheng, X. Zhang, K. Uvdal, *Cryst. Growth Des.* **2012**, *12*, 2707 – 2713.
[31] I. Sheikhshoaie, Z. Tohidiyana, *CJBAS* **2015**, *3*, 164–170.
[32] C.S. Lee, C. Y. Wu, W. S. Wen-Shu Hwang, J. Dinda, *Polyhedron* **2006**, *25*, 1791–1801.
[33] S. Singh, K. Pal, *Mater. Des.* **2015**, *82*, 223–237.
[34] K. Nakamoto, *Infrared and Raman Spectra of Inorganic and Coordination Compounds Part B 5th Edn.*, John Wiley & Sons, NY, **1997.**
[35] J. R. Ferraro, W. R. Walker, *Inorg. Chem.* **1965**, *4*, 1382–1386.
[36] T. D. Smith, J. R. Pilbrow, *Coord. Chem. Rev.* **1974**, *13*, 173–278.
[37] B. Kozlevčar, I. Leban, I. Turel, P. Šegedin, M. Petrić, F. Pohleven, A. J. P. White, D. J. Williams, J. Sieler, *Polyhedron* **1999**, *18*, 755–762.
[38] J. Moncol, M. Korabik, P. Seglá, M. Koman, D. Mikloš, J. Jašková, T. Glowiak, M. Melník, J. Mrozinski, M. R. Sundberg. *Z. Anorg. Allg. Chem.* **2007**, *633*, 298–305.
[39] P. L. Holland, W. B. Tolman, *J. Am. Chem. Soc.* **2000**, *122*, 6331–6332.
[40] R. A. Shiekh, I. A. Rahman, M. A. Malik, N. Luddin, S. M. Masudi, S. A. Al-Thabaiti, *Int. J. Electrochem. Sci.* **2013**, *8*, 6972–6987.
[41] G. S. Caravajal, D. E. Leyden, G. R. Quinting, G. E. Maciel, *Anal. Chem.* **1988**, *60*, 1776–1786.
[42] L. He, Y. Xiong, M. Zhao, X. Mao, Y. Liu, H. Zhao, Z. Tang, *Chem. Asian. J.* **2013**, *8*, 1765–1767
[43] F. Zuo, S. Yan, B. Zhang, Y. Zhao, Y. Xie, *J. Phys. Chem. C* **2008**, *112*, 2831–2835.
[44] B. Zhang, X. Ye, W. Dai, W. Hou, Y. Xie, *Chem. Eur. J.* **2006**, *12*, 2337–2342.
[45] B. L. Banik, P. Fattahi, J. L. Brown, *Nanomed. Nanobiotechnol.* **2016**, *8*, 271–299.
[46] J. P. Rao, K. E. Geckeler, *Prog. Poly. Sc.* **2011**, *36*, 887–917.
[47] Y. Xia, Z. Tang, *Chem. Commun.* **2012**, *48*, 6320.
[48] Y. Xia, Z. Tang, *Adv. Funct. Mater.* **2012**, *22*, 2585.
[49] A. Karmakar, L. M. D. R. S. Martins, S. Hazra, M. F. C. Guedes da Silva, A. J. L. Pombeiro, *Cryst. Growth Des.* **2016**, *16*, 1837–1849.
[50] M. Sharma, B. Das, G. V. Karunakar, L. Satyanarayana, K. K. Bania, *J. Phys. Chem. C* **2016**, *120*, 13563–13573.
[51] P. Deka, R. C. Deka, P. Bharali, *New J. Chem.* **2016**, *40*, 348–357.
[52] P. Deka, A. Hazarika, R. C. Deka, P. Bharali, *RSC Adv.* **2016**, *6*, 95292–95305.

Submitted: September 7, 2016
Accepted: December 2, 2016